

An assessment of structural enthalpy and crystallization pathways of $\text{Mg}_{65}\text{Zn}_{30}\text{Ca}_5$ bulk metallic glass and amorphous films

Scott Gleason, David Miskovic, Nicholas Hamilton, Kevin Laws, Michael Ferry

UNSW Australia
School of Material Science and Engineering

August 2, 2017

ABSTRACT

The structural nature and thermal stability of amorphous alloys is highly dependent on the method by which they are produced, i.e. their relaxation rate upon cooling. Both bulk samples and metallic glass films of $\text{Mg}_{65}\text{Zn}_{30}\text{Ca}_5$ were produced by copper mold casting and direct current (DC) magnetron sputtering onto aluminium substrates, respectively. Comparisons between structural enthalpy, crystallization pathways, relaxation and crystallization kinetics of the bulk samples and films were examined by elevated temperature XRD and DSC. Compared with equivalent experiments on the bulk alloy, results for the thin films show distinct differences in structural enthalpy and deviations from the expected crystalline phase evolution, displaying minor peak shifts, failure of some phases to evolve, and variations in the evolution rates.

TABLE OF CONTENTS

ABSTRACT	i
TABLE OF CONTENTS	1
1 INTRODUCTION	1
2 METHOD	1
2.1 Master alloy	1
2.2 DC magnetron sputtering	1
2.3 Stylus profiler analysis	2
2.4 EDS analysis	2
2.5 DSC characterization	2
2.6 XRD characterization	2
3 RESULTS	3
3.1 Alloy composition	3
3.2 DSC	3
3.2.1 Isothermal DSC	3
3.2.2 Fragility	3
3.3 DSC deconvolution	3
3.3.1 Onset determination	3
3.3.2 Reaction enthalpy	5
3.3.3 Relaxation enthalpy	5
3.4 XRD	5
3.4.1 Annealing XRD	5
3.4.2 Dynamic XRD	5
4 DISCUSSION	5
5 CONCLUSIONS	5
6 ACKNOWLEDGEMENTS	5
7 REFERENCES	5

1 INTRODUCTION

The structural nature and thermal stability of amorphous alloys is highly dependent on the method by which they are produced, i.e. their relaxation rate upon cooling. Both bulk samples and metallic glass films of $\text{Mg}_{65}\text{Zn}_{30}\text{Ca}_5$ were produced by copper mold casting and direct current (DC) magnetron sputtering onto aluminium substrates, respectively. Comparisons between structural enthalpy, crystallization pathways, relaxation and crystallization kinetics of the bulk samples and films were examined by elevated temperature XRD and DSC. Compared with equivalent experiments on the bulk alloy, results for the thin films show distinct differences in structural enthalpy and deviations from the expected crystalline phase evolution, displaying minor peak shifts, failure of some phases to evolve, and variations in the evolution rates.

Key sources ^{Zhang Zhang Zhang 2012} [1, 2] [3]

2 METHOD

2.1 Master alloy

The master alloy of $\text{Mg}_{65}\text{Zn}_{30}\text{Ca}_5$ was produced using high-purity elements of Mg (99.85 wt%), Zn (99.995 wt%), and Ca (99.8 wt%). The alloy was prepared by induction melting in boron nitride coated graphite crucibles, purged with Ar (99.997 vol.% purity) five times, and protected with a circulating Ar atmosphere. Alloy homogeneity was ensured by heating and cooling through a cycle of 700°C, 385°C, 650°C, 385°C, 650°C to a casting temperature of 500 °C and 450°C for injection and gravity casting respectively. Bulk amorphous $\text{Mg}_{65}\text{Zn}_{30}\text{Ca}_5$ rods of 2.5mm diameter and plates of thickness of $XX\mu\text{m}$ were produced by copper mold injection casting. The 25.4mm diameter targets were prepared from a cylindrical copper mold gravity castings sectioned to thicknesses of 3.25mm. All samples and targets were stored under Ar when not being examined or used.

2.2 DC magnetron sputtering

Films were produced from an in-house DC magnetron sputtering facility with Ar working gas (99.997 vol.% purity). The power was 15W, typical voltage of 290 – 350V, nominal chamber pressure of 1 bar, substrate temperature of 25°C, and Ar flow of 3.01 SCCM. Films were deposited directly onto to Al DSC lid substrates. Depositions were for a period of 35 minutes. Deposition rate was estimated at 1.2nm/s.

2.3 Stylus profiler analysis

Nominal film thickness was measured by a stylus profiler (Dektak 2A, Bruker, Germany). A glass slide was placed under the substrates within the sputtering chamber, allowing the substrates to act as a mask. Profile measurements were taken by measuring the height difference between the bare glass and the film coated glass. This film thickness was used to estimate the sputter deposition rate.

2.4 EDS analysis

Alloy composition and homogeneity were confirmed by SEM-EDS (S3400, Hitachi, Japan). Hyper-maps were collected with an accelerating voltage of 15 – 20 kV, and a probe current of 50 μ A. (Conditions; counts were 5000 kps or better, dead time was less than 20 %, and working distance was 10 mm).

2.5 DSC characterization

Isochronic DSC (204 F1 Phoenix, Netzsch, Selb, Germany) was carried out in Al crucibles under a protective Ar atmosphere (99.997 vol.% purity). Scans were performed at heating rates of 5 to 100 K/min.

For annealed XRD the samples were heat treated in the DSC by heating to the desired temperature at 20 K/min followed by Ar quenching to room temperature.

2.6 XRD characterization

Annealing XRD (Empyrean, PANalytical, Cu K_{α} X-ray source, $\lambda = 1.541 \text{ \AA}$) was performed at room temperature. (Generator Voltage 45, Tube Current 40, Scan Step Size 0.0262606, Time per Step 397.29).

Dynamic XRD (D8, Bruker, Cu K_{α} X-ray source, $\lambda = 1.541 \text{ \AA}$) was performed by raising temperature at a rate of 20 K/min and performing scans *in situ*. The first scan was performed at 35°C, then 75°C, after which temperature was raised in 5 K increments until reaching the peak temperature at 185°C. The 2θ scans from 31 – 60° were completed within 1092 sec (18 min, 12 sec) to minimise the effects of recrystallisation during the experiment. (Generator Voltage 45, Tube Current 100, Scan Step Size 0.02, Time per Step 134.4).

3 RESULTS

3.1 Alloy composition

From the 35 minute depositions a nominal film thickness of $2.5\mu\text{m}$ was obtained, giving a deposition rate of approximately 1.2nm/s . The temperature within the chamber was found to rise $3 - 4^\circ\text{C}$, significantly less than the expected 20K suggested by similar setups [4].

EDS analysis shows good agreement in the nominal composition for both the bulk and film $\text{Mg}_{65}\text{Zn}_{30}\text{Ca}_5$, see Table 1.

EDS Analysis	Bulk (at%)	Film (at%)
Mg	64.85 ± 3.18	62.92 ± 3.24
Zn	29.55 ± 0.82	31.17 ± 0.95
Ca	5.60 ± 0.17	5.91 ± 0.19

Table 1: EDS composition of bulk and film $\text{Mg}_{65}\text{Zn}_{30}\text{Ca}_5$ in atomic weight percent.

3.2 DSC

3.2.1 Isothermal DSC

3.2.2 Fragility

Variable heating rate DSC for both the bulk and film $\text{Mg}_{65}\text{Zn}_{30}\text{Ca}_5$ was used to establish the fragility of the system. Numerical solutions were used to fit the equation $\beta^{-1} = \tau_0 e^{\left(\frac{D^*T_0}{T-T_0}\right)}$ [5] for both the bulk and film. The fragility m could then be calculated from the relationship $D^* = 590/(m - 16)$ [6, 7].

For the bulk it was found $\beta^{-1} = 1.338E - 16e^{5274\left(\frac{1}{T-T_0}\right)}$ with Adj. $R^2 = 0.972$, giving a $D^* = 20.4$, and a fragility $m = 44.9$. For the film $\beta^{-1} = 5.921E - 11e^{2766\left(\frac{1}{T-T_0}\right)}$ with Adj. $R^2 = 0.861$, giving a $D^* = 10.0$, and fragility $m = 75.0$. See Figure 3.

3.3 DSC deconvolution

3.3.1 Onset determination

Both the bulk and film $\text{Mg}_{65}\text{Zn}_{30}\text{Ca}_5$ were examined at various DSC heating rates to observe changes in the T_g and T_x temperatures. As expected higher heating rates resulted

endothermic peaks shifting to higher temperatures and curve convolution.

Numerical solutions were used to deconvolution the DSC data so the various T_x onsets could be determined. The results of the deconvolution are presented in Table 2 for the bulk and Table 3 for the film.

Heating Rate β <i>K/min</i>	T_g	T_{x1}	T_{x2}	T_{x3}	T_{x4}	T_{x5}
100	136.1	164.8	193.4	201.8	240.2	262.4
80	132.0	160.0	194.4	201.9	238.2	260.3
60	129.6	157.7	190.0	197.8	232.9	259.0
40	126.6	155.2	189.0	200.0	226.4	254.7
30	126.2	151.5	187.0	198.4	221.0	251.1
20	125.1	149.8	188.4	197.0	216.0	246.8
15	123.8	148.3	186.2	195.6	212.2	243.9
10	123.5	144.5	183.4	192.9	207.4	239.8
5	120.5	141.1	179.7	187.5	199.8	232.7

Table 2: Bulk $\text{Mg}_{65}\text{Zn}_{30}\text{Ca}_5$ alloy onset temperatures for the various DSC heating rates β . All temperatures are in $^{\circ}\text{C}$.

Heating Rate β <i>K/min</i>	T_g	T_{x1}	T_{x2}	T_{x3}	T_{x4}	T_{x5}
100	108.5	128.6		177.3		240.3
80	106.0	121.2		165.6		238.8
60	107.3	134.0		176.1		237.8
40	100.2	119.8		170.7		234.2
30	95.3	110.4		169.5		232.5
20	95.5	115.2		170.5		229.4
15	92.5	113.5		168.8		224.0

Table 3: Film $\text{Mg}_{65}\text{Zn}_{30}\text{Ca}_5$ alloy onset temperatures for the various DSC heating rates β . All temperatures are in $^{\circ}\text{C}$.

3.3.2 Reaction enthalpy

3.3.3 Relaxation enthalpy

3.4 XRD

3.4.1 Annealing XRD

3.4.2 Dynamic XRD

4 DISCUSSION

The use of a 60K DSC heating rate compared to the more commonly used 20K rate [sources] shifts peaks for the bulk $\text{Mg}_{65}\text{Zn}_{30}\text{Ca}_5$ alloy about 8 - 15 degrees higher. This higher heating rates were used because crystallization events for the films were difficult to differentiation at the lower heating rate. Films show little shift to high temperature peaks with increases heating rates, but large shifts with relaxation. Bulk show the opposite behaviour, larger peaks shifts with higher heating rates and little shift with relaxation.

5 CONCLUSIONS

6 ACKNOWLEDGEMENTS

Yu Wang for his assistance with XRD experimentation and Rietveld refinement.

7 REFERENCES

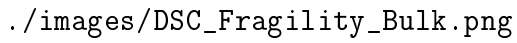
hang2013

[1] Y. N. Zhang, G. J. Rocher, B. Briccoli, D. Kevorkov, X. B. Liu, Z. Altounian, and M. Medraj. Crystallization characteristics of the Mg-rich metallic glasses in the Ca-Mg-Zn system. *Journal of Alloys and Compounds*, 552:88–97, 2013.

hang2012

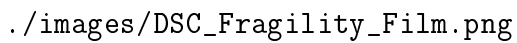
[2] Yi-Nan Zhang, Dmytro Kevorkov, Xue Dong Liu, Florent Bridier, Patrice Chartrand, and Mamoun Medraj. Homogeneity range and crystal structure of the $\text{Ca}_2\text{Mg}_5\text{Zn}_{13}$ compound. *Journal of Alloys and Compounds*, 523:75–82, 2012.

- hang2011 [3] Yi-Nan Zhang, Dmytro Kevorkov, Florent Bridier, and Mamoun Medraj. Experimental study of the Ca-Mg-Zn system using diffusion couples and key alloys. *Science and Technology of Advanced Materials*, 12(2):025003, 2011.
- Wang2014 [4] J. Q. Wang, N. Chen, P. Liu, Z. Wang, D. V. Louzguine-Luzgin, M. W. Chen, and J. H. Perepezko. The ultrastable kinetic behavior of an Au-based nanoglass. *Acta Materialia*, 79(0):30–36, 2014.
- usch1998 [5] R. Busch, W. Liu, and W. L. Johnson. Thermodynamics and kinetics of the Mg₆₅Cu₂₅Y₁₀ bulk metallic glass forming liquid. *Journal of Applied Physics*, 83(8):4134–4141, 1998.
- gell2002 [6] C. A. Angell and S. Borick. Specific heats C_p , C_v , C_{conf} and energy landscapes of glassforming liquids. *Journal of Non-Crystalline Solids*, 307 - 310:393–406, 2002.
- Wei2014 [7] Shuai Wei, Zach Evenson, Isabella Gallino, and Ralf Busch. The impact of fragility on the calorimetric glass transition in bulk metallic glasses. *Intermetallics*, 55:138–144, 2014.

The figure shows a plot of DSC curves for bulk Mg₆₅Zn₃₀Ca₅ sample. The plot area is mostly blank, with the file path visible at the bottom.

./images/DSC_Fragility_Bulk.png

Figure 1: Bulk Mg₆₅Zn₃₀Ca₅ relaxed at 120 °C for 10 minutes and heated at various heating rates. The insert stacks the differential scanning calorimetry (DSC) curves and labels the T_g and T_x es of the 100K/min sample.

The figure shows a plot of DSC curves for film Mg₆₅Zn₃₀Ca₅ sample. The plot area is mostly blank, with the file path visible at the bottom.

./images/DSC_Fragility_Film.png

Figure 2: Unrelaxed film Mg₆₅Zn₃₀Ca₅ heated at various heating rates. The insert stacks the DSC curves and labels the T_g and T_x es of the 100K/min sample.

./images/Bulk_Film_Fragility.png

Figure 3: Fitted fragility for the $\text{Mg}_{65}\text{Zn}_{30}\text{Ca}_5$ system obtained by DSC at various heating rates

m_mValue



Figure 4: DSC deconvolution for the bulk. From left to right, top to bottom, 5, 10, 15, 20, 30, 40, 60, 80, 100 K/min.



Figure 5: DSC deconvolution for the film. From left to right, top to bottom, 15, 20, 30, 40, 60, 80, 100 K/min.

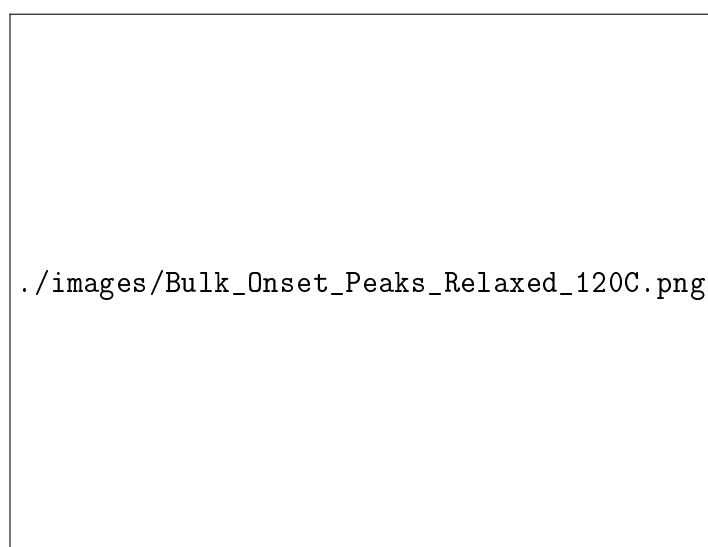


Figure 6: The T_g s and T_x es of the bulk $Mg_{65}Zn_{30}Ca_5$ at all heating rates.

./images/Onsets_BulkandFilm.png

Figure 7: The T_g s and T_x es of the bulk and film $\text{Mg}_{65}\text{Zn}_{30}\text{Ca}_5$ at all heating rates.

./images/Decon_Onsets_BR.png

./images/Decon_peak_area_BR.png

Figure 8: DSC onset temperatures and enthalpy of formation for the bulk and film.

./images/XRD_Annealing_Bulk.png

Figure 9: XRD pattern for Bulk $\text{Mg}_{65}\text{Zn}_{30}\text{Ca}_5$ heated through several crystallization peaks identified from DSC

./images/XRD_Annealing_Film.png

Figure 10: XRD pattern for Film $\text{Mg}_{65}\text{Zn}_{30}\text{Ca}_5$ heated through several crystallization peaks identified from DSC

./images/XRD_Dynamic_Bulk.png

(a)

./images/Bulk_Heated_XRD_Waterfall3D_Smooth2.png

(b)

Figure 11: (a) Stacked X-ray diffraction (XRD) patterns from the incremental heating of bulk $\text{Mg}_{65}\text{Zn}_{30}\text{Ca}_5$. (b) Cascading XRD patterns from the incremental heating of bulk $\text{Mg}_{65}\text{Zn}_{30}\text{Ca}_5$.

amic_FullStack_Film

./images/XRD_Dynamic_Film.png

(a)

amic_WaterFall_Film

./images/TF_Facet_HeatXRD_Waterfall3D_Smooth.png

(b)

mic_Film

Figure 12: (a) Stacked XRD patterns from the incremental heating of film $\text{Mg}_{65}\text{Zn}_{30}\text{Ca}_5$. (b) Cascading XRD patterns from the incremental heating of film $\text{Mg}_{65}\text{Zn}_{30}\text{Ca}_5$.